Journal of Materials Chemistry A

The energetics of phosphoric acid interactions reveals a new acid loss mechanism

Journal:	*Journal of Materials Chemistry A*
Manuscript ID	TA-ART-02-2019-001756.R1
Article Type:	Paper
Date Submitted by the Author:	15-Mar-2019
Complete List of Authors:	Lee, Albert; Los Alamos National Laboratory Choe, Yoong-Kee; National Institute of Advanced Industrial Science and Technology Matanovic, Ivana; University of New Mexico Kim, Yu Seung; Los Alamos National Laboratory

SCHOLARONE™
Manuscripts

ARTICLE

The energetics of phosphoric acid interactions reveals a new acid loss mechanism

Received 00th January 20xx,
Accepted 00th January 20xx

DOI: 10.1039/x0xx00000x

Albert S. Lee,[a]† Yoong-Kee Choe,[b]† Ivana Matanovic[c,d] and Yu Seung Kim[a]*

Acid retention of phosphoric acid (PA)-doped proton exchange membranes (PEMs) is one of the critical factors that determine the durability of high temperature PEM fuel cells. However, the mechanism of PA loss in the PEMs in the presence of water is obscure in the context of the energetics of the PA cluster. Here, we study the energetics of PA-benzimidazole acid-base and biphosphate-ammonium ion pairs using density functional theory calculations and ^{31}P NMR experiments to propose a novel PA loss mechanism. The results suggest that the removal of the PA from the membrane does not occur due to the strong interaction of PA-water, but due to the incapability of the base polymers to hold the water and PA beyond a certain level. Significantly higher interaction in the biphosphate-ammonium ion pair shifts the equilibrium PA composition in the PA cluster to higher values, which minimizes the PA loss in the presence of water. Introducing the high interaction with PA molecules provides a path for better PEM design that may allow using high temperature PEM fuel cells with excellent acid retention.

Introduction

Low temperature proton exchange membrane fuel cells (LT-PEMFCs) that use a water-based sulfonated polymer membrane are currently the leading technology for automotive fuel cell applications.[1] The LT-PEMFCs operate at 60-90 °C with high power density and durability. However, the relatively low operating temperature makes waste heat rejection into the environment difficult, particularly in hotter surroundings, which poses a significant challenge for water and heat management.[2] High temperature PEMFCs (HT-PEMFCs) that use phosphoric acid (PA)-doped polybenzimidazole (PBI) can operate at temperatures above 100 °C without humidification and resolve the waste heat rejection issue.[3-5] However, PA loss during fuel cell cold start-ups and lower temperature operations makes the HT-PEMFC unsuitable for automotive applications.[6] Furthermore, PA loss of HT-PEMFCs at normal operating temperatures, ca. 160-180 °C remains a significant challenge for long-term fuel cell operation.[7-9]

Over several decades, several acid loss mechanisms for PA-PBI have been investigated to improve the PA retention in HT-PEMFCs. Mori et al. first proposed the acid absorbance mechanism from phosphoric acid fuel cells in the late 1980s.[10] According to this mechanism, acid loss occurs due to the fuel cell electrodes that absorb PA. In the early 2000s, Li et al. observed that some PA molecules in the PBI remained after immersion in methanol and they hypothesized that PA loss occurs by liquid water which washes out the free acid from highly doped PA-PBI, i.e., acid leaching mechanism.[11] In 2006, Yu et al. observed that PA loss rate from the cathode effluent was 80 ng /cm^2 h at 190 °C, which was ~10 times higher than the PA loss rate at 160 and 80 °C (~7.5 ng /cm^2 h).[12] Based on observation, they proposed the steam distillation mechanism according to which PA is distilled out with high water vapor pressure. This mechanism may explain well the high PA loss at 190 °C, but it is not consistent with relatively high PA loss rate at 80 °C. More recently, our research group suggested that PA loss may occur because the interaction between PA and water is stronger than the interaction of the acid-base, which makes PA molecules segregate from the membrane in the presence of water.[13]

Previous PA loss mechanisms described the physical aspects of the PA loss under specific conditions without considering the energetics of PA interacting with the base functional group. Here, we investigate the energetics of PA interaction with two base functional groups, i.e., benzimidazole (BI) and tetramethyl ammonium hydroxide (TMA) to propose a new PA loss mechanism. The proposed mechanism is explained by the equilibrium composition of PA and water of two PA-doped polymers, i.e., PA-PBI and biphosphate-quaternized ammonium (biphosphate-QAP) at various relative humidity (RH) levels. PA retention at high RHs and temperature was examined. Fuel cell performance of membrane electrode assemblies (MEAs) using biphosphate-QAP provides a path for PEM design in advanced HT-PEMFC systems.

[a] *MPA-11: Materials Synthesis & Integrated Devices, Los Alamos National Laboratory, Los Alamos, New Mexico 87545, USA*
[b] *National Institute of Advanced Industrial Science & Technology, Tsukuba 305-8568, Japan*
[c] *Department of Chemical and Biological Engineering, Center for Micro-Engineered Materials (CMEM), The University of New Mexico, Albuquerque, New Mexico 87231, USA*
[d] *Theoretical Division, Los Alamos National Laboratory, Los Alamos, New Mexico 87545, USA*
† These authors contributed equally to this work.
Electronic Supplementary Information (ESI) available: [Tables S1-4]. See DOI: 10.1039/x0xx00000x

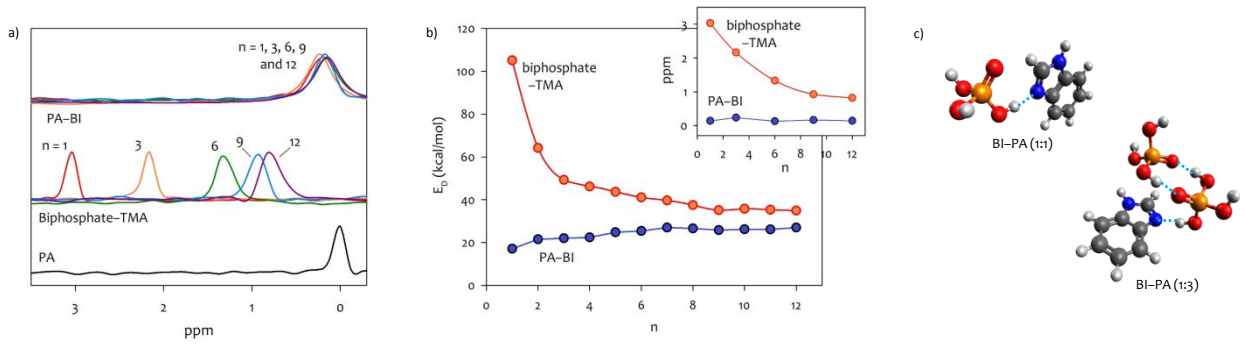

Fig. 1. (a) ^{31}P NMR spectra of PA (n·H_3PO_4)-BI and biphosphate (H_2PO_4 (n-1)·H_3PO_4)-TMA as a function of the number of PA (n); (b) Decomposed interaction energy, E_D, of PA-BI and biphosphate-TMA as a function of n; the inset figure shows the chemical shift of ^{31}P NMR from **Fig. 1a**; (c) Optimized structure of the cluster consisting of one BI + one PA and one BI + three PAs. Blue dotted lines indicate hydrogen bonds (Color description: Carbon: Grey, Oxygen: Red, Nitrogen: Blue, Phosphorous: Orange, Hydrogen: White).

Result and Discussion

Energetics of anhydrous PA-benzimidazole and PA-TMA complex

The energetics of PA complexes is investigated using ^{31}P NMR in which the shift of the NMR chemical peak to higher frequencies (downfield) indicates the interaction strength in the PA cluster. Fig. 1a shows the ^{31}P NMR spectra of anhydrous PA-BI and biphosphate-TMA as a function of the number of PA. The chemical peak of the PA-BI is broader than that of PA because the proton from PA is coupled with BI. The slight chemical shift of the PA-BI, ca. 0.2 ppm suggests a weak acid-base interaction between PA and BI. The chemical shift of the PA-BI is invariant to the number of PA in the system, indicating that the interaction strength of the PA does not change with the number of PA molecules. This result suggests that the strength of the acid-base interaction is similar to that of hydrogen bonding interaction between PAs. This is expected as the interaction between two PAs is of acid-base nature. For the anhydrous biphosphate-TMA, we note three differences as compared to PA-BI. First, the chemical peak width for the PA-TMA cluster is narrower than that of the PA-BI cluster. This can be attributed to the strong basicity of quaternary ammonium hydroxide, which causes complete PA deprotonation (proton decoupling) and forms a biphosphate anion-quaternary ammonium cation pair. Second, the downfield shift of the chemical peaks for the biphosphate-TMA is more significant than that for the PA-BI at a given number of PA. Third, the chemical shift of the biphosphate-TMA gradually decreases as the number of PA increases, suggesting that the interaction of biphosphate-TMA weakens with additional PA molecules.

To understand the energetics of the PA clusters in the two systems, we used Density Functional Theory (DFT) to calculate the decomposed binding energy, E_D as a function of the number of PA (Table S1 and Fig. 1b). For PA-BI, the E_D slightly increases from 17.1 to 25.4 kcal/mol as the number of PA increases from 1 to 5 and then becomes constant, ~26 kcal/mol, which is consistent with the ^{31}P NMR result. The increase in the binding energy of the PA-BI cluster with respect to the number of PA reflects the increase in the number of hydrogen bonds in the cluster when the number of PA increases. Fig. 1c shows optimized structure of BI + one PA and BI + two PAs. As can be seen, the number of hydrogen bonds increases when going from BI + one PA to BI + two PAs. Our results show that the PA-BI acid-base interaction is slightly lower than the PA-PA hydrogen bonding interaction, which is consistent with previously calculated hydrogen bonding energy of acid-base pair and two PA molecules. Safonova et al. reported the acid-base interaction energy of 14.7-19.4 kcal/mol between dimethylformamide and PA using different levels of theory.[14,15] Paddison et al. reported ZPE- and BSSE-corrected interaction energy between two PAs as 24.9 and 20.6 kcal/mol, respectively at the B3LYP/6-311G** level.[16] They also indicated that E_D of the PA molecule clusters slightly increased as the number of PA increased. This result indicates that the term “free acid,” used by many researchers, may be misleading as it suggests that the free acid is easy to leach out.[17-20]

For biphosphate-TMA, the binding energy per PA exponentially decays from 105.1 to 34.9 kcal/mol as the number of PA increases from 1 to 12. The exponential decay of E_D for biphosphate-TMA is due to the relatively large interaction energy change by sharing the negative charge of the biphosphate with the additional PA molecules. However, it is important to note that even at the association of 12 PA molecules, the E_D value is notably higher for the ion pair system than for the acid-base system (34.9 vs. 27 kcal/mol). The trend of the E_D change for the two PA complex systems is in good agreement with the chemical shift of the ^{31}P NMR results (see inset of Fig. 1b). The DFT results also show that the ionic interaction in biphosphate-TMA pair (1:1) is significantly higher, > 6 times than the acid-base interaction in PA-BI pair (1:1).

Impact of water on the energetics of the PA complex

Next, the impact of water on the energetics of the PA-BI and biphosphate-TMA is investigated. Fig. 2 shows that the chemical peaks of the ^{31}P NMR for both PA-BI and biphosphate-TMA systems, further shift to downfield when 10 water molecules were added to the PA-BI and biphosphate-TMA (1:1). The chemical shift for the PA-BI is 2.2 ppm, significant downfield shift, ca. 2.0 ppm, from that of the anhydrous PA-BI, suggesting that substantially increased the cluster interaction energy. The biphosphate-TMA exhibited a much smaller shift, ca. 0.07 ppm, from that of the anhydrous biphosphate-TMA.

This journal is © The Royal Society of Chemistry 20xx

Please do not adjust margins

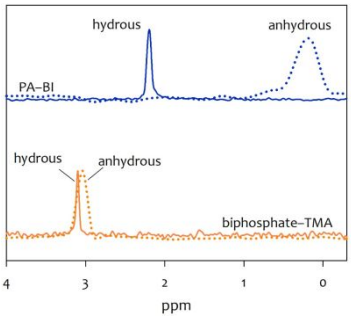

Fig. 2. (a) ^{31}P NMR spectra comparison between hydrous and anhydrous PA-PBI (1:1) and biphosphate-TMA (1:1); the water to PA ratio is 10.

The interaction in the hydrous clusters, $\Delta E_{base\text{-}PA\text{-}water}$ as a function of the number of water molecules is calculated using DFT calculations (Table 1). As the results show, the interaction energy between (PA + H_2O) and BI increases with the incorporation of water. With adding one water molecule, the interaction energy increases from 17.1 to 18.5 kcal/mol. With adding five water molecules, the interaction energy increases to 39.9 kcal/mol, more than twice to that of anhydrous PA-BI. With adding ten water molecules, the interaction energy becomes 36.5 kcal/mol, slightly lower than the PA-BI with five water molecules. The DFT illustrates the optimized structure of BI + PA + nH_2O (n =1, 5, 10) clusters (Fig. 3a). In the case of BI with one PA and one water molecule, a hydrogen bond between the PA + H_2O cluster and BI is formed at one site (one of the nitrogen atoms of BI and the hydrogen atom of PA). For the other clusters, two hydrogen bonds are formed between the base and the water.[21] The increased energetics values in Table 1 therefore reflect an increase in the number of hydrogen bonds between the base and the cluster. Since the number of the available hydrogen bonds are the same for n = 5 or 10, the interaction energy for both clusters is similar.

Table 1. Interaction energy of base-PA-water (1-1-n) cluster.

$\Delta E_{base\text{-}PA\text{-}n\ water}$	*n*			
	0	1	5	10
PA-BI	17.1	18.5	39.9	36.5
Biphosphate-TMA	105.1	106.5	105.2	113.2

The increase in the interaction energy of biphosphate-TMA is relatively small; with adding ten water molecules, the interaction energy increases for only ~ 8%. This can be attributed to the fact that in TMA there are no atoms that can serve as hydrogen bond donors, which is in contrast to BI (Fig. 3b). In addition, it is difficult for the nitrogen atom of TMA to form a hydrogen bond due to the steric hindrance of several methyl groups around it. As such, additional water molecules in the hydrous biphosphate-TMA are not able to interact through the hydrogen bond with TMA. The high interaction energy, as mentioned above, found in biphosphate-TMA systems arises from the ionic interaction between TMA cation and biphosphate anion. Lower cluster energy with an increased amount of PA explains well the PA loss in a commercial PBI based HT-PEMFCs in which the acid evaporation rates are higher at the beginning of the life than after long-term operation.[12]

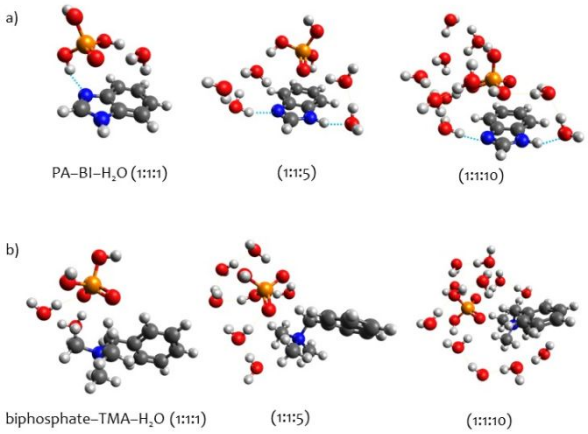

Fig. 3. Optimized structure of the cluster consisting of (a) BI-PA-water and (b) TMA-biphosphate-water. Blue dotted lines indicate hydrogen bonds between the base and PA + water cluster. Other hydrogen bonds are not shown for clarity. (Color description: Carbon: Grey, Oxygen: Red, Nitrogen: Blue, Phosphorous: Orange, Hydrogen: White).

The impact of the number of PA on the cluster interaction energy of the hydrous PA complex is shown in Fig. 4. For both the hydrous PA-BI and biphosphate-TMA, the interaction energy gradually decreases as the number of PA increases, different from those of the anhydrous systems; the interaction energy of anhydrous PA-BI is almost invariant, and the interaction energy of anhydrous biphosphate-TMA decreases exponentially with the PA molecules.

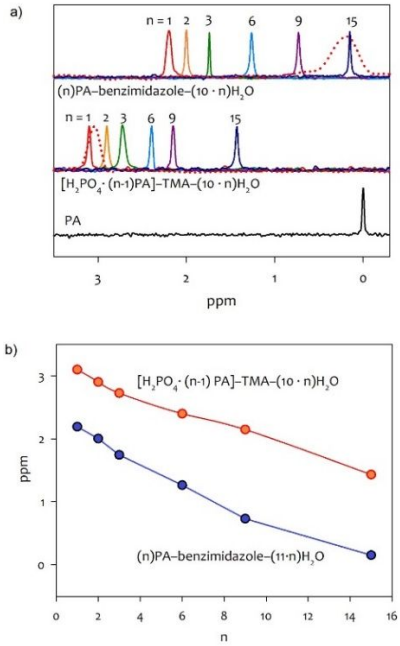

Fig. 4. (a) ^{31}P NMR spectra of hydrous PA-BI (n · H_3PO_4-BI-(10 · n) · H_2O) and biphosphate-TMA (H_2PO_4 · (n-1) · H_3PO_4-TMA-(10 · n) · H_2O) as a function of n. (b) Interaction energy of hydrous PA-BI (n · H_3PO_4-BI-(10 · n) · H_2O) and biphosphate-TMA (H_2PO_4 · (n-1) · H_3PO_4-TMA-(10 · n) · H_2O) as a function of n.

Please do not adjust margins

Proposed PA loss mechanism of PA-doped PEMs

The energetics of the PA-BI and biphosphate-TMA cluster does not support the presumptions of the previous PA loss mechanism in two aspects. First, the energetics analysis indicates that the PA-BI interaction is not significantly higher than the hydrogen bonding interactions between PAs in the cluster. This is in stark contrast with conventional sulfonated membranes in which the ionic interaction between the sulfate anion and hydronium cation is significantly higher than the hydrogen bonding (acid-base) interaction between the water molecules. Namely, in the LT-PEMFC membranes, the acid cluster interactions gradually decrease as the number of water increases and the state of the water can be classified as tightly bonded, loosely bonded, and free water.[22] However, in the PA-PBI membrane, the difference in the interaction energy between PA-BI and two PAs is small, so the state of PA is not well defined as bonded PA and free PA. Our DFT calculations suggest that the interaction energies of the PA-BI clusters with the first five PAs are even lower than those associate with more PA molecules. In the presence of water, the interaction of PA-BI reduces as the number of PA molecules increases. However, the energetic state of free PA is only achieved with a very high number of PA, i.e., 14 per BI instead of 2 as proposed from the acid leaching mechanism.[11] As PA loss can occur with a relatively low number of PA molecules, the PA loss does not correlate well with the amount of free acid. Second, the cluster interaction of the PA-BI increases with adding first two water molecules and maintains similar value with additional water molecules. For example, the decomposed interaction energy of anhydrous PA-BI (9:1) is ~ 25.8 kcal/mol, and the cluster energy further increases with incorporating water as evidenced by further downfield chemical shift (2 ppm) of the ^{31}P NMR spectra. Considering that the interaction energy of PA-water is only 12.6 kcal/mol,[13] adding water into the PA complex system cannot remove PAs from the system. This is also evidenced by the single peak of the ^{31}P NMR, which suggests that there is no PA segregation with adding water to the PA complex. This result refutes the idea that water weakens the interaction of PA-BI and biphosphate-TMA.

The energetic study using small model compounds indicated that the membrane with more PA should have at least same stability, which is the opposite of what occurs in the PA-PBI membrane system. This result suggests that the PA loss must be related to the polymer matrix as well as the energetics between the base functional group and water. Namely, the PA loss mechanism should be understood by the membrane capability to hold high number of PA molecules. This mechanism is similar to the solvent desorption process of the ion exchange membranes.[23] When an exchange membrane is exposed to a single-solvent, the membrane starts to adsorb the solvent. The solvent uptake is determined by the interaction (or affinity) between the ionic functional group and solvent molecules as well as by the polymer properties such as chain rigidity or phase structure. When the solvent-swollen membrane is exposed to the dry condition, solvent desorption process occurs to reach the new thermodynamic equilibrium. If the membrane contains multiple solvents, the solvent composition in the membrane is determined by the partition equilibrium. Likewise, the PA composition for PA-doped membranes is determined by the equilibrium partition between water and PA and polymer capability to hold the PA and water molecules. Since normal HT-PEMFC operates under anhydrous conditions, the concentration of water is below the equilibrium partition and PA loss is insignificant. However, when water activity increases, the water concentration increases to reach the equilibrium partition. Further increase of water activity changes the equilibrium partition toward water-rich composition and results in substantial PA loss from the system.

Fig. 5 schematically illustrates the proposed PA loss mechanism compared to the previous PA loss mechanism. According to the previous PA loss mechanism, when a PA-PBI membrane is exposed to water (I), the water molecules from the environment penetrate to the PA cluster of PA-PBI and take "loosely bound" PA molecules out of the membrane (PA leaching). Subsequent exposure of the membrane to a higher temperature, ca. > 100 °C (II), causes water molecules in the PA phase to start moving out of the membrane, leaving "strongly bound" PA molecules. This mechanism contradicts with the energetics of PA cluster, as adding water increases the interaction of the PA clusters. In the proposed PA loss mechanism, when a PA-PBI membrane is exposed to water (I), the water molecules from the environment keep adding to the PA cluster phase until the PA cluster cannot hold more water due to the physical constraint of the rigid polymer chains. Since the PA cluster interaction energy is greatly increased with adding water, some PA molecules are exchanged with water molecules to reach a new equilibrium partition composition (PA loss). Subsequent exposure of the membrane to a higher

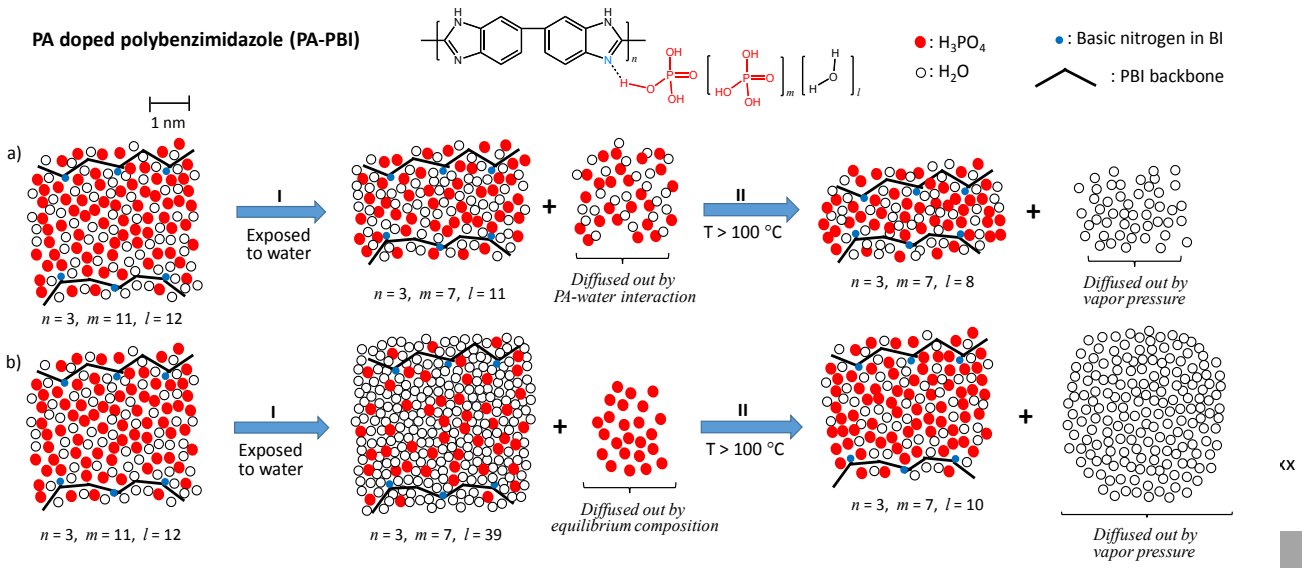

Fig. 5. Schematic illustration of (a) previous PA loss mechanism and (b) proposed PA loss mechanism during subsequent exposure to water and high temperature (> 100 °C)

temperature, ca. > 100 °C (II), causes the water molecules in the PA phase to start escaping the membrane as the water vapor pressure exceeds the hydrogen bonding of water in the PA cluster.

One distinctive difference between these two mechanisms is the volume change of the PA cluster upon exposure to water. Since the past mechanism hypothesized that water-PA interaction is higher than the PA cluster interaction energy, the adsorbed water molecules form a strong bond with PA which makes the PA molecules diffuse out of the membrane. In this case, most of the water adsorbed in the membrane leach out PA molecules decreasing the volume of the PA cluster. This process would cause volume of the PA cluster to decrease or stay the same. In contrast, according to the proposed mechanism, the size of the PA cluster would increase because a more significant amount of water would be added compared to lost PA molecules in favor of increasing the cluster interaction energy until the membrane cannot hold more water due to the physical restriction.

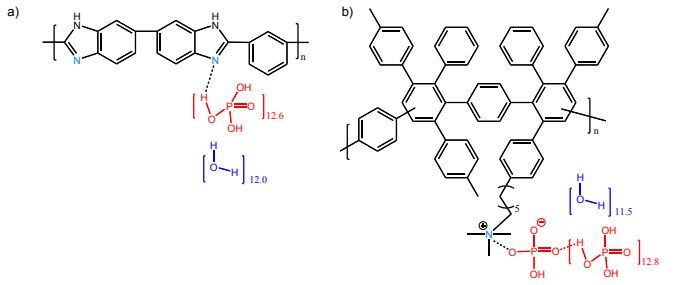

Fig. 6. Chemical structures of PA-PBI and biphosphate-QAP

Experimental validation and implication for fuel cells

To validate the proposed PA loss mechanism, we prepared two polymeric systems, *i.e.*, commercially available PA-PBI and biphosphate-ammonium ion pair coordinated polymer (biphosphate-QAP) prepared from aryl ether-free quaternary ammonium poly(phenylene)[28,29] (Fig. 6). Both polymer systems have rigid backbone structures without aliphatic components in the polymer backbone. The PA-PBI has a high concentration of benzimidazole base (6.5 meq./g) while the concentration of ammonium hydroxide base in biphosphate-QAP is much smaller (1.9 meq./g). Both PEMs were prepared from the imbibing process using 85% aqueous PA solution. The number of PA molecules per base after the imbibing process are comparable (12.6 for PA-PBI and 13.8 for biphosphate-QAP). The comparable number of PA molecules per base in spite of much higher interaction of biphosphate-QAP than PA-PBI is attributed the higher base concentration of PBI, which allows more PA molecules via polymer plasticization.

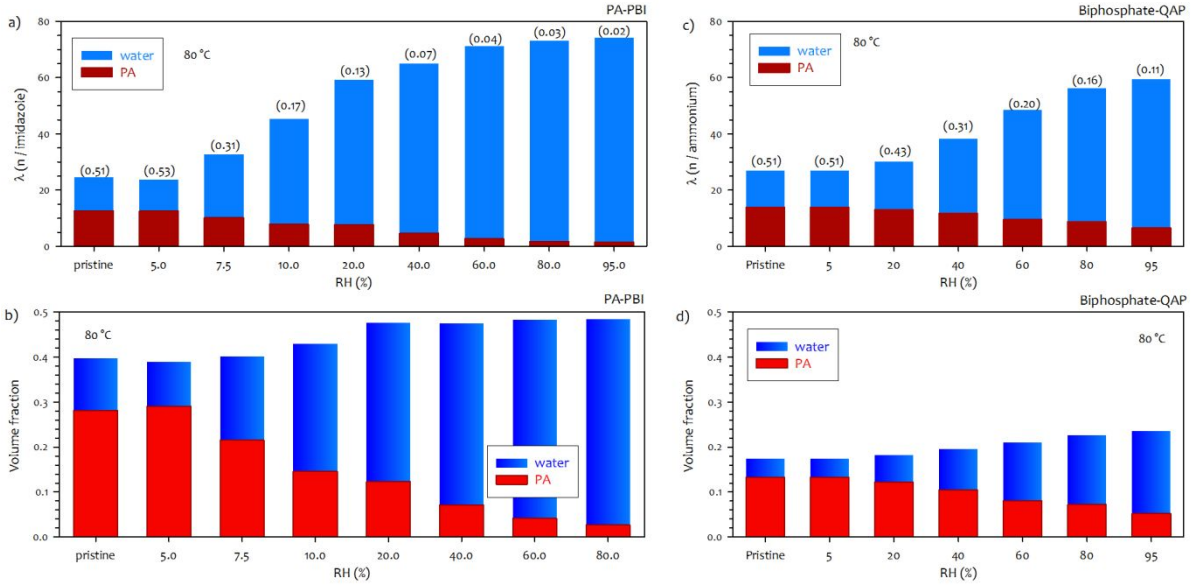

Fig. 7. The equilibrium number of PA and water molecules per base for (a) PA-PBI and (b) biphosphate-QAP as a function of RH at 80 °C. The values for pristine sample were obtained after the imbibing process. (b) The volume fraction of PA and water for (c) PA-PBI and (d) biphosphate-QAP as a function of RH at 80 °C.

The proposed mechanism explains well why PA loss from PA-PBI fuel cell is negligible at the optimum operating temperature, ca. 160-180 °C in spite of water generating conditions.[12,24-27] From the viewpoint of previous PA loss mechanism, "free PA" should diffuse out quickly upon contact with vapor water. However, from the viewpoint of the proposed PA loss mechanism, PA loss upon contact with vapor water will not occur as long as the membrane can hold the water molecules below the equilibrium partition composition.

Fig. 7a shows the equilibrium uptake of PA and water in PA-PBI as a function of RH at 80 °C. As the RH increases, the total number of PA and water molecules in the PA-PBI membrane increases because the number of absorbed water molecules is

much higher than the number of desorbed PA molecules. For example, the 40 water molecules per BI was added to the PA cluster while only 5 PA molecules per BI diffused out when the RH changed from 5 to 20 %. Accordingly, the volume fraction of the PA cluster of PA-PBI increases from 0.39 to 0.48 (Fig. 7b). The increased water molecules in the membrane can be explained with the PA cluster energetics we used to support the proposed PA loss mechanism. Another note from the sorption experiment is the change of the absorbed water molecule from the pristine (after the imbibing process) to 80 °C, 5% RH. As seen in Fig. 7a, the PA-PBI membrane only lost 0.7 water molecules per BI after 18 hours at 80 °C, 5 % RH, indicating that the PA complex energy in the PA-PBI membrane is high.

Compared to PA-PBI, the biphosphate-QAP membrane has a higher composition of PA at a given RH, because the ionic interaction in the biphosphate-QAP is higher than the acid-base interaction in the PA-PBI (Fig. 7c). For example, the biphosphate-QAP retains 11.7 PA molecules per quaternary ammonium while the PA-PBI retains only 4.6 PA molecules per BI at 40 % RH. The volume fraction of PA complex cluster of biphosphate-QAP also increased as the RH increased (Fig. 7d), suggesting that the biphosphate-QAP membrane has the same PA loss mechanism. Lower change in the PA volume fraction compared to PA-PBI is due to the higher ion pair interaction in the cluster as opposed to acid-base interaction in the PA-PBI system. It is also noted that the overall volume fraction of PA and water molecules inside the membrane is much higher for PA-PBI. This may be attributed to the much higher overall PA content in the PA-PBI system which allows plasticizing the polymer backbone to accommodate more PA and water molecules in the PA-PBI.

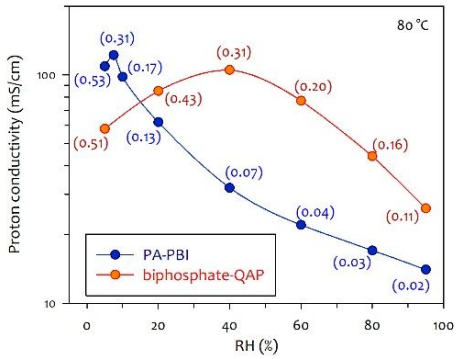

Fig. 8. Equilibrium proton conductivity of PA-PBI and biphosphate-QAP as a function of RH. The numbers in parenthesis is the PA fraction in the PA cluster.

We further investigated the impact of the PA fractional change on proton conductivity. Fig. 8 compares the proton conductivity of the two membranes as a function of RH. At 5% RH, the proton conductivity of PA-PBI is 109 mS/cm. As the RH increases to 7.5%, the proton conductivity of PA-PBI increases to 122 mS/cm, then exponentially decreases with further RH increase. The proton conductivity of biphosphate-QAP increases from 58 mS/cm at 5% RH to ~ 100 mS/cm at 40% RH. The proton conductivity decreases with further RH increases. The maximum conductivity for both PA-PBI and biphosphate-QAP was obtained at the PA to water ratio of 0.31 which is in good agreement with previously reported experimental results.[30] At a similar level of PA to water ratio, PA-PBI has higher conductivity than biphosphate-QAP, presumably due to the higher total number of the PA and water in the membrane. Important note from this experiment is the RH that shows the maximum value, in which the HT-PEMFC can be operated stably. The RH showing the maximum conductivity for PA-PBI is 7.5%, but the biphosphate-QAP has much higher RH, i.e., 40%. This result indicates much higher water tolerance for the biphosphate-QAP system.

The temperature effect on PA and water loss was examined (Fig.9). As the temperature increases from 80 to 120 °C, both system loses water mostly. Further increase in the temperature, relatively small amount of PA is also lost. PA-PBI exhibiting a higher overall water and PA loss across all temperatures. For example, at 120 °C, PA-PBI loses ~4.1 water molecules per base which constitutes a ~33% loss of its initial water content, while bisphosphate-QAP loses only about half of that (~2.1 mol water/base), corresponding to a mere ~15.3% loss of its initial water content. At 200 °C, PA-PBI lost 4.4 PA molecules, while biphosphate-QAP lost 1.3 PA molecules. The higher retention of water and PA in the biphosphate-QAP system is due to the higher cluster energy shown in Table 1.

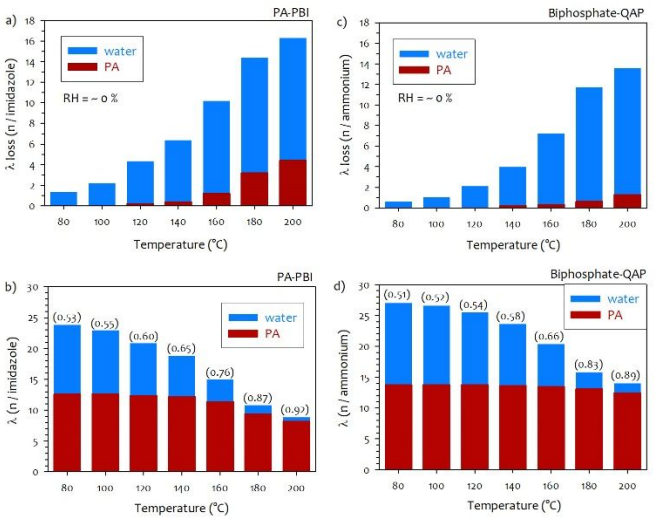

Fig. 9. The effect of temperature on PA and water loss. (a) PA and water loss of (c) PA-PBI and (b) biphosphate-QAP and equilibrium PA and water content of (b) PA-PBI and (d) biphosphate-QAP

This journal is © The Royal Society of Chemistry 20xx

Please do not adjust margins

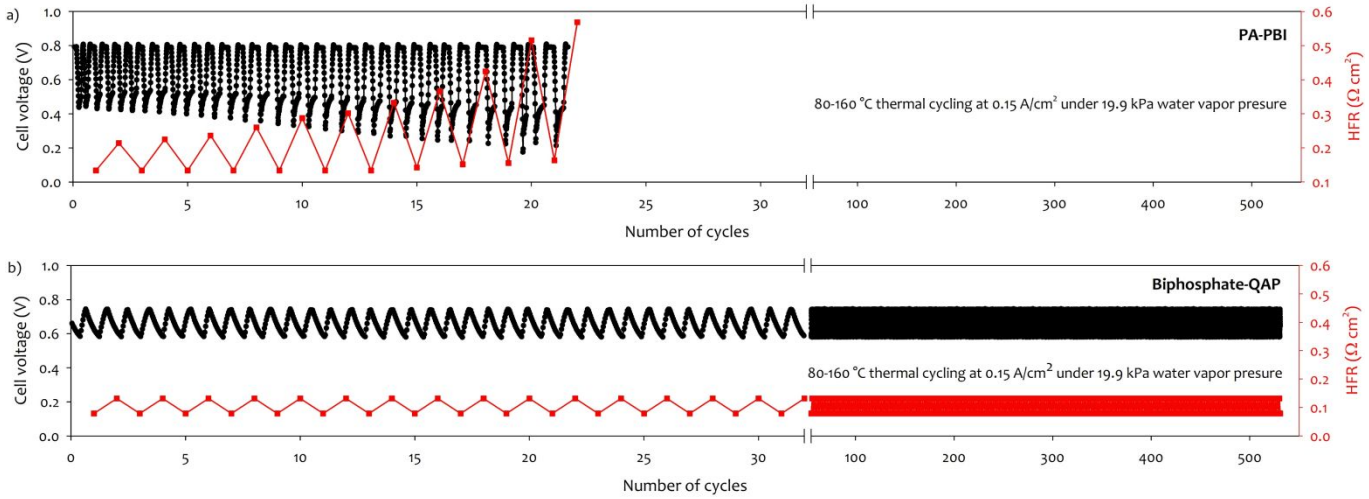

Fig. 10. Cell voltage change during thermal cycling of fuel cells under constant current density of 0.15 A/cm² and partial water vapour pressure of 19.9 kPa. The cell voltage was measured at backpressure of 10 psi.

The impact of the PA fractional change at different RH levels on the water tolerance of fuel cell performance is shown in Fig. 10. Short-term stability of MEAs employing the PA-PBI and biphosphate-QAP membranes was evaluated during the thermal cycling between 80-160 °C under a constant current density of 150 mA/cm^2 and constant water vapor pressure of 19.9 kPa. The water vapor pressure corresponds to 42% RH at 80 °C. In this thermal cycling test, cell voltage changes due to the catalytic activity changes by cell temperature. For the PA-PBI fuel cell, the cell voltage gradually decreased and the fuel cell stopped running after 23 cycles. The cell high frequency resistance (HFR) of the MEA increased over 3 fold (from 0.14 to 0.55 Ω cm^2), which is consistent with the conductivity result (3.6 times lower conductivity when the RH changes from ~ 5 to 40 % at 80 °C (Fig. 8).

For the biphosphate-QAP fuel cell, the voltage variation at the operating temperature of 80-160 °C is smaller. The higher high-limit voltage of 0.78 V (vs. 0.79 V for PA-PBI fuel cell) was due to the lower anhydrous conductivity of the biphosphate-QAP membrane, while the low-limit voltage was 0.59 V (vs. 0.41 V for PA-PBI fuel cell) due to the higher hydrous conductivity of the biphosphate-QAP membrane, which can partially compensate for the cell performance loss of the low operating temperature. The performance of the biphosphate-QAP fuel cell was stable (~530 cycles) until we stopped the test. Polarization curves before and after the thermal cycling tests reveal drastic differences in the PA-PBI and biphosphate-TMA membrane systems (Fig. S5). While the PA-PBI membrane system exhibited significant ohmic loss manifested as a three-fold loss in peak power density and approximately three-fold increase in HFR after only 23 thermal cycles, the biphosphate-TMA system only lost about ~9% loss in peak power density after ~530 thermal cycles with almost no change in HFR.

Both the stable cell voltage and HFR suggest that the biphosphate-QAP membrane maintains PA fraction in the PA complex cluster high enough (> 0.3) during the thermal cycling test under constant partial water vapor pressure.

Conclusions

We propose a new PA loss mechanism based on the energetics of PA clusters in the presence of water. This energetic study suggests that adding water in the PA cluster increases the cluster interaction energy. A new PA loss mechanism based on the energetics is explained: PA loss occurs with the equilibrium compositional change of PA and water in the physically confined cluster volume. The proposed mechanism is verified by measuring the volume change of the PA-PBI as a function of RH. The proposed PA loss mechanism is not only consistent with the energetics of PA complex in PA-PBI, but is also the only mechanism that can explain the reason why PA-PBI fuel cells have minimal PA loss at 160-180 °C in the presence of water from the cathode. The proposed mechanism suggests that the PA retention of the PA-PBI membranes may be enhanced by increasing the PA cluster energy. Several researchers reported higher PA retention by introducing hydrogen bonding with silica[31-33] and ionic interaction.[34-36]

An alternative and potentially more efficient way to increase the interaction energy of the PA cluster and enhance the PA retention would be to replace the benzimidazole with quaternary ammonium group. The model compound study using biphosphate-ammonium TMA ion pairs indicates that the equilibrium composition can shift to the higher PA composition due to the much stronger ionic interaction as opposed to the acid-base interaction found in PA-PBI. This result suggests that ion-pair coordinated PEMs can be stably run even in the presence of water without PA loss. The thermal cycling fuel cell tests under the constant water vapour pressure of 19.9 kPa demonstrate that the biphosphate-QAP membrane has excellent water tolerance. This study provides insights for the design of new PEM that can be used under partially hydrated fuel cell operating condition which has been a bottleneck for current PBI-based high temperature PEMs.

This journal is © The Royal Society of Chemistry 20xx

Please do not adjust margins

Experimental

Materials

85 wt% phosphoric acid (PA) (Sigma Aldrich, 99.99%), tetramethylammonium hydroxide pentahydrate, $TMAOH{\cdot}5H_2O$ (Sigma Aldrich, 99%), 1,3-benzimidazole, BI (Sigma Aldrich, 98%), anhydrous magnesium sulfate, $MgSO_4$ (Sigma Aldrich, 99.5%), and dimethyl sulfoxide, DMSO-d_6 (Cambridge Isotope Lab, 99.9%) were all used as received. Polybenzimidazole (PBI) membranes were purchased from PBI Performance Plastics. Quaternary ammonium functionalized polymers (QAPs) were provided from Sandia National Laboratories.

^{31}P NMR measurement

For the anhydrous ^{31}P NMR measurements, a commercial 85 wt% phosphoric acid aqueous solution (4 g, 34.6 mmol equivalent of phosphoric acid) was added to anhydrous DMSO-d_6 (0.525 ml) was added to a glass vial. The solution was chilled using cold-water bath and 250 mg of anhydrous $MgSO_4$ as dehydrating agent was quickly added. Heat evolution was observed due to the exothermic dehydration process. After storing the solutions overnight, $MgSO_4$ was syringe filtered into another pre-dried vial, where either $TMAOH{\cdot}5H_2O$ or BI was added. After sonication for 10 min to dissolve the base, the solution was injected into a dry NMR glass tube and sealed immediately prior to analysis. For the hydrated ^{31}P NMR samples, a commercial 85 wt% phosphoric acid aqueous solution (4 g, 34.6 mmol equivalent of phosphoric acid) was diluted to 10 M using D_2O. To this solution, corresponding amounts of either $TMAOH{\cdot}5H_2O$ or BI was added and sonicated until completely dissolved. This solution was directly used for NMR analysis. A Bruker Advance 500 MHz NMR spectrometer was used with resonant frequencies of ^{1}H: 500 MHz and ^{31}P: 202 MHz. Spectra were recorded in either DMSO-d_6 or D_2O at 25 °C.

Computational Details

All of the calculations were carried out using the Gaussian 16 quantum chemistry package.[37] For geometry optimization and frequency calculations, we employed density functional theory (DFT) with M06-L functional.[38] 6-31G(d) basis set was used for all atoms. Density fitting approximation was used for all the calculations where we used auto keyword in the Gaussian program to automatically generate density fitting sets.[39,40] The clusters of the base + multiple PA or the base + PA + multiple water molecules are constructed by randomly placing multiple PA or water molecules around the base. Geometry optimization were conducted for the cluster and vibrational frequency calculations were carried on the optimized structure to ensure that the optimized structure is not a saddle point. We have not carried out details analysis to check whether the optimized structure represents the global minimum structures. As such, optimized structure reported herein is likely to be a local minimum.

The decomposed binding energy, E_D, was calculated from the binding energy, ΔE_{Base}. The binding energy indicates the difference between the energy of the cluster and the sum of the energy of its constituent molecules as shown in eq. 1.[16]

$$\Delta E_{base} = \{\text{Base} + n\ \text{H}_3\text{PO}_4\} - \{\text{Base} + n \times \text{free}\ \text{H}_3\text{PO}_4\}$$ (Base = BI or TMA+OH$^-$) (1)

For example, ΔE_{BI} of the cluster composed of six PAs and one BI is computed to be 152.4 kcal/mol while that composed of one PA and one BI is computed to be 17.1 kcal/mol. The magnitude of ΔE_{base} is roughly proportional to the number of available hydrogen bonds in the clusters (Table S1). In the case of TMA, TMA is paired with one OH- and OH- abstracts one proton from PA to form H_2O, if PA is located close to it. Thus, for the cluster composed of TMA and PA, one PA always exits as dihydrogen phosphate (H_2PO_4-) due to OH-. The decomposed binding energy, E_D is calculated by dividing the binding energy by the number of PA (eq. 2) for both PA-BI and biphosphate-TMA where the state of the hydrogen bonded PAs and the ionic biphosphate is non-distinguishable due to the fast electron transfer between the PAs and biphosphate.

$$E_D = \frac{\Delta E_{base}}{n}\ (n = 1\text{–}12) \quad (2)$$

The interaction in the hydrous clusters, $\Delta E_{\text{base-PA-water}}$ as a function of the number of water molecules is calculated using the following equation:

$$\Delta E_{\text{base}-\text{PA}-\text{water})} = \{\text{BI (or TMA)} + \text{H}_3\text{PO}_4 + \text{H}_2\text{O}\} - \{\text{BI (or TMA)} + (\text{H}_3\text{PO}_4 + n\ \text{H}_2\text{O})\} \quad (3)$$

$\Delta E_{\text{base-(PA+water)}}$ indicates the interaction between the base and the PA + water cluster and the calculated values are given in Table 1. To calculate $\Delta E_{\text{base-(PA+water)}}$, clusters composed of Base + PA + water were fully optimized. After the optimization, a single point energy calculation was carried out without the base molecule where geometrical parameters of PA + water were fixed to the ones obtained by the geometry optimization of the whole cluster. These calculations result in the energetics of the PA + water cluster.

Equilibrated water and PA content and proton conductivity of polymer electrolytes

PBI and QAP membranes were doped in 85 wt% phosphoric acid aqueous solution for over 10 h at room temperature and excess phosphoric acid wiped away via blotting with dry kimwipe. Afterwards, multiple membrane samples were hung from a glass rod with a paper clip and subjected to prolonged exposure at 5 to 95% RH at 80 °C. Two concurrent conductivity window cells with PA-PBI and biphosphate-QAP membranes was also subjected to the same humidity conditions and multiple AC impedance measurements over a minimum of 24 hrs was monitored to determine the equilibriated state of the RH condition. Once the membranes were equilibriated at each RH condition, the membrane samples were taken out and immediately weighed with a microbalance to measure the membrane's weight in its doped, hydrated state, $\text{Weight}_{\text{wet}}$ and thus to calculate the total uptake of the dope, $\text{Uptake}_{\text{total}}$ by subtracting it from the dry membrane, $\text{Weight}_{\text{dry}}$. It is worthy to note that for the initial $\text{Weight}_{\text{dry}}$ membranes of 0.1 g, the

This journal is © The Royal Society of Chemistry 20xx

Please do not adjust margins

standard error range of $Uptake_{total}$ is approximately 2 mg for each measurement. Each run was done at least twice for verification of $Uptake_{total}$. Specific values measured are shown in Table S2.

With the corresponding membranes sampled at each equilibriated RH condition, acid-base titrations were carried out to calculate the phosphoric acid content. Briefly, the membrane was completely submerged in 100 ml of deionized water with 3 drops of methyl orange indicator dye solution (pre-made 3 wt% in deionized water) and stirred magnetically for approximately 1 h. To this solution, 0.5 ml aliquots of 0.1 M NaOH standard solution was added until color change from orange to yellow was observed. The phosphoric acid content in total weight, $Weight_{PA}$ from these experiments was calculated from the following equation 4:

$$Weight_{PA} = (V_{NaOH} \times C_{NaOH}) / (Equiv_{mol}) \times FW_{PA} \quad (4)$$

where V_{NaOH} is the volume of NaOH, C_{NaOH} is the molar concentration of NaOH (0.1 M), $Equiv_{mol}$ is the equivalent mol of acid (3 in this case), and FW_{PA} is the formula weight of phosphoric acid (98 g/mol).

As the above $Uptake_{total}$ value is a measure of the sum of phosphoric acid and water uptake, $Weight_{PA}$ and $Weight_{H2O}$, respectively, the difference between $Uptake_{total}$ and $Weight_{PA}$ was used to backcalculate $Weight_{H2O}$. The λ values (the number of water and PA per base groups) reported in Fig. 4 were calculated from the water uptake and PA uptake using the following equations 5 and 6, where IEC is the ion exchange capacity in mmol / g. Note the IEC values for PBI and QAP used in this study were 6.5 and 1.9 mmol / g, respectively.

$$\lambda_{PA} = (Weight_{PA} / FW_{PA}) / (IEC/1000) \quad (5)$$
$$\lambda_{H2O} = (Weight_{H2O} / FW_{H2O}) / (IEC/1000) \quad (6)$$

The values for each calculated value are shown in Table S3. The volume fraction was also calculated by the following equations:

$$\text{Volume fraction of PA} = (Vol_{PA} / Vol_{dry} + Vol_{H2O}) \quad (7)$$
$$\text{Volume fraction of } H_2O = (Vol_{H2O} / Vol_{dry} + Vol_{PA}) \quad (8)$$

where both the Vol of PA and water were calculated from the $Weight_{PA}$ and $Weight_{H2O}$ values in Table S3 along with the formula weights (FW) and densities (δ) of water and phosphoric acid using the general equation Vol = Weight x FW / d. Table S4 tabulates the values for the volume fraction. Note that the densities for dry PBI and QAP were measured to be 1.3 and 1.18 g /cm^3, respectively.

For the temperature-dependent water and PA evaporation experiments, the PA-PBI and biphosphate-QAP membranes were treated at the corresponding temperature under anhydrous conditions for 18 h. The same calculations of λ_{PA} and λ_{H2O} were used as for the relative humidity-dependent experiments.

Fuel cell durability

Membrane electrode assemblies fabricated with PA-PBI and biphosphate-QAP membranes and standard gas diffusion electrodes identically prepared with our previous study[13] were subjected to a thermal accelerated stress test (AST). In this thermal AST, we measured the cell voltage change as the temperature is cycled between 80-160°C at a constant heating/cooling rate of 10°C/min and constant current of 0.15 A/cm^2 under H_2/O_2 flow rate of 500 sccm, partial water vapour pressure of 19.9 kPa. The HFR measurements were conducted when the temperature reached 80 or 160 °C.

Conflicts of interest

There are no conflicts to declare.

Acknowledgements

We thank Dr. C. Fujimoto for providing quaternized polymer samples. Y.-K Choe acknowledges financial support from the Ministry of Economy, Trade and Industry of Japan. This work was supported by the U.S. Department of Energy (US DOE), Energy Efficiency and Renewable Energy (EERE), Fuel Cell Technologies Office (FCTO) under Contract Number 89233218CNA000001.

Notes and references

1 A. Kongkanand and M.F. Mathias, *J. Phys. Chem. Lett.* 2016, **7**, 1127.
2 R.K. Ahluwalia and X.H. Wang, *J. Power Sources*, 2008, **177**, 167.
3 Q. Li, J.O. Jensen, R.F. Savinell and N.J. Bjerrum, *Prog. Polym. Sci.*, 2019, **34**, 449.
4 A. Chandan, M. Hattenberger, A. El-kharouf, S. Du, A. Dhir, V. Self, B.G. Pollet, A. Ingram and W. Bujalski, *J. Power Sources*, 2013, **13**, 264.
5 S. Bose, T. Kuila, T.X.H. Nguyen, N.H. Kim, K.-T. Lau and J.H. Lee, *Prog. Polym. Sci.*, 2011, **36**, 813.
6 S. Lang, T.J. Jazdal, F. Kuhl and M.J. Hampe*, Int. J. Hydrog. Energy*, 2015, **40**, 1163.
7 S.H. Eberhardt, T. Lochner, F.N. Buchi and T.J. Schmidt, *J. Electrochem. Soc.*, 2015, **40**, 1163.
8 S.H. Eberhardt, M. Toulec, F. Marone, F.N. Buchi and T.J. Schmidt, *J. Electrochem. Soc.*, 2015, **162**, 1367.
9 T. Sondergaard, L.N. Cleemann, H. Becker, T. Steenberg, H.A. Hjuler, L. Seerup, Q. Li and J.O. Jensen, *J. Electrochem. Soc.*, 2018, **165**, 3053.
10 T. Mori, A. Hongi, T. Kahara and Y. Hishinuma, *J. Electrochem. Soc.*, 1988, **135**, 1104.
11 Q. Li, R. He, R.W. Berg, H.A. Hjuler and N.J. Bjerrum, *Solid State Ionics*, 2004, 168, 177.
12 S. Yu, L. Xiao and B.C. Benicewicz, *Fuel Cells*, 2008, 8, 165.
13 K.S. Lee, J.S. Spendelow, Y.-K. Choe, C. Fujimoto and Y.S. Kim, *Nature Energy*, 2016, **1**, 1.
14 M.A. Krest'yaninov, M.G. Kiselev and L.P. Safonova, *Russ. J. of Phys. Chem. A*, 2012. **86,** 1847.
15 E.A. Khatuntseva, M.A. Krest'yaninov, I.V. Fedorova, M. Kiselev and L. Safonova, *Russ. J. of Phys. Chem. A*, 2015, **89,** 2248.

16 L. Vilciauskas, S.J. Paddison and K.D. Kreuer, *J. Phys. Chem. A*, 2009, **113**, 9193.
17 J. Lobato, P. Carizares, M.A. Rodrigo, J.J. Linares and F.J. Pinar, *Int. J. Hydrog. Energy*, 2010, **35**, 1347.
18 C. Xu, Y. Cao, R. Kumar, X. Wu, X. Wang and K. Scott, *J. Mater. Chem*., 2011, **21**, 11359.
19 A. Sannigrahi, S. Ghosh, S. Maity and T. Jana, *Polymer*, 2011, **52**, 4319.
20 G.A. Giffin, S. Galbiati, M. Walter, K. Aniol, C. Ellwein, J. Kerres and R. Zeis, *J. Membrane Sci.*, 2017, **535**, 122.
21 P. Musto, P.L. Manna, J.D. Moon, M. Galizia and B.D. Freeman, *ACS Omega*, 2018, **3**, 11592.
22 Y.S.Kim, L. Dong, M.A. Hickner, T.E. Glass, V. Webb and J.E. McGrath, *Macromolecules*, 2003, **36**, 6281.
23 P.W. Majsztrik, M.B. Satterfield, A.B. Borcarsly, J.B. Beniger, *J. Membrane Sci.*, 2007, **301**, 93.
24 F.J. Pinar, P. Canizares, M.A. Rodrigo, D. Ubeda, J. Lobato, *J. Power Sources*, 2011, **196**, 4306.
25 H.J. Lee, B.G. Kim, D.H. Lee, S.J. Park, Y. Kim, J.W. Lee, D. Henkensmeier, S.W. Nam, H.-J. Kim, H. Kim and J.-Y. Kim, *Int. J. Hydrog. Energy*, 2011, **36**, 5521.
26 C. Wannek, B. Kohnen, H.-F. Oetjen, H. Lippert and J. Mergel, *Fuel Cells*, 2008, **8**, 87.
27 S. Galbiati, A. Baricci, A. Casalegno and R. Marchesi, *Int. J. Hydrog. Energy*, 2013, **38**, 6469.
28 M.R. Hibbs, *J. Polym. Sci. Part B-Polym. Phys*., 2013, **51**, 1736.
29 E.J. Park, and Y.S. Kim, *J. Mater. Chem. A*, 2018, **6**, 15456.
30 D.-T. Chin, H.H. Chung, *J. Appl. Electrochem.*, 1989, **19**, 95.
31 P. Mustarelli, E. Quatarone, S. Grandi, A. Carollo and A. Magistris, *Adv. Mater.*, 2008, **20**, 1339.
32 Y.J. Kuo and H.L. Lin, *Int. J. Hydrog. Energy*, 2018, **43,** 4448.
33 Y. Ozdemir, N. Uregen and Y. Devrim, *Int. J. Hydrog. Energy*, 2017, **42**, 2648.
34 S. Maity, S. Singha and T. Jana, *Polymer*, 2015, **66**, 76.
35 F.X. Liu, S. Wang, H. Chen, J. Li, X. Tian, X. Wu, T. Mao, J. Xu and Z. Wang, *ACS Sus. Chem. Eng*., 2018, **6**, 16352.
36 B. Lin, G. Qiao, F. Chu, S. Zhang, N. Yuan and J. Ding, *RSC Adv.*, 2017, **7**, 1056.
37 M.J.T. Frisch, G. Wu, H.B. Schlegel, G.E. Scuseria, M.A. Robb, J.R. Cheeseman, G. Scalmani, V. Barone, B. Mennucci, G.A. Petersson, H. Nakatsuji, M. Caricato, X. Li, H.P. Hratchian, A. Izmaylov, J. Bloino, G. Zheng, J.L. Sonnenberg, M. Hada, M. Ehara, K. Toyota, R. Fukuda, J. Hasegawa, M. Ishida, T. Nakajima, Y. Honda, O. Kitao, H. Nakai, T. Vreven, J.A. Montgomery, J.E. Peralta, F. Ogliaro, M. Bearpark, J.J. Heyd, E. Brothers, K.N. Kudin, V.N. Staroverov, R. Kobayashi, J. Normand, K. Raghavachari, A. Rendell, J.C. Burant, S.S. Iyengar, J. Tomasi, M. Cossi, N. Rega, J.M. Millam, M. Klene, J.E. Knox, J.B. Cross, V. Bakken, C. Adamo, J. Jaramillo, R. Gomperts, R.E. Stratmann, O. Yazyev, A.J. Austin, R. Cammi, C. Pomelli, J. Ochterski, R.L. Martin, K. Morokuma, V.G. Zakrzewski, G.A. Voth, P. Salvador, J.J. Dannenberg, S. Dapprich, A.D. Daniels, O. Farkas, J.B. Foresman, J.V. Ortiz, J. Cioslowski, D.J. Fox, *Gaussian 16, Revision A. 03*. 2016, Gaussian, Inc.: Wallingford CT.
38 Y. Zhao D.G. Truhlar, *J. Chem. Phys.*, 2006. **125**, 194101.
39 B.I. Dunlap, *J. Chem. Phys.*, 1983, **78**, 3140.
40 B.I. Dunlap, B.I., *J. Mol. Struc.-Theochem*, 2000, **529**, 37.

This journal is © The Royal Society of Chemistry 20xx

Please do not adjust margins

Table of Content

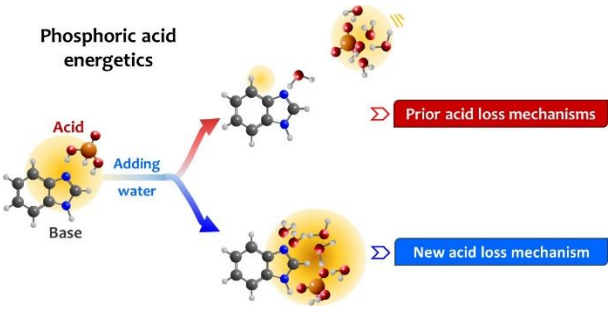

The energetics of acid-base interaction suggests a new acid loss mechanism that allows developing advanced membranes for fuel cells.